# On the Time-Temperature-Transformation Behavior of a New Dual-Superlattice Nickel-Based Superalloy

P.M. MIGNANELLI, N.G. JONES, M.C. HARDY, and H.J. STONE

Recent research has identified compositions of nickel-based superalloys with microstructures containing appreciable and comparable volume fractions of $\gamma'$ and $\gamma''$ precipitates. In this work, an alloy capable of forming such a dual-superlattice microstructure was subjected to a range of thermal exposures between 873 K and 1173 K (600 °C and 900 °C) for durations of 1 to 1000 hours. The microstructures and nature of the precipitating phases were characterized using synchrotron X-ray diffraction and electron microscopy. These data have enabled the construction of a T-T-T diagram for the precipitating phases. Hardness measurements following each thermal exposure have identified the age-hardening behavior of this alloy and allowed preliminary mechanical properties to be assessed.

DOI: 10.1007/s11661-017-4355-8


## I. INTRODUCTION

RECENT trends in nickel-based superalloy design have primarily focused upon the development of new materials for the highest temperature applications. However, the continued use of Inconel 718 (IN718) in intermediate to high temperature regimes, on account of its excellent mechanical strength and processability, suggests that opportunities still exist for new high-strength nickel-based superalloys with temperature capabilities beyond that of IN718.[1–4]

IN718 derives the majority of its strength from gamma double prime ($\gamma''$) precipitates, which possess the $D0_{22}$ structure (Strukturbericht notation).[5] Conversely, the A1 gamma ($\gamma$) matrices of higher temperature nickel-based superalloys are strengthened by gamma prime ($\gamma'$) precipitates, which possess the $L1_2$ structure. The $L1_2$ and $D0_{22}$ structures are superlattice structures of the A1 matrix[6] and are able to form coherent interfaces with the matrix. This compatibility of the lattices confers considerable strengthening through order hardening, especially at high temperature.[7] Importantly, the $\gamma''$ produces mechanical property benefits that are in excess of the $\gamma'$ phase on a per volume fraction basis, due to the large coherency strains associated with the $\gamma''$ precipitates.[8] However, the benefits of $\gamma''$ reinforcing precipitates cannot be exploited in alloys operating at the highest temperatures, as the $\gamma''$ is known to be a metastable phase.[9,10] Consequently, the $\gamma''$ transforms to the thermodynamically stable $\delta$ phase during prolonged exposure at elevated temperatures.[11] The inability to stabilize the $\gamma''$ phase through alloying or microstructural modification has resulted in the almost exclusive use of the $\gamma'$ phase as the reinforcing precipitate of the most recent high-temperature nickel-based superalloys.

As IN718 is the most commonly used $\gamma''$ reinforced superalloy, consisting of ~20 pct $\gamma''$ and ~3 pct $\gamma'$, extensive research has been performed to understand its temperature capability and the stability of the $\gamma''$ phase.[12–15] Such studies have identified that the metastable nature of the $\gamma''$ precipitates limits operational temperatures to <923 K (650 °C).[16,17] International research seeking to increase the temperature capability of $\gamma''$ reinforced alloys has predominantly focused on small modifications to the composition of IN718 to improve the stability of the $\gamma'$ and $\gamma''$ phases and retard the onset of $\delta$ formation.[18,19] An increase in temperature capability was achieved by increasing the (Al + Ti)/Nb ratio, along with the Al/Ti ratio, and culminated in the design of the alloy Ticolloy.[20,21] The improved stability and greater volume fraction of $\gamma'$ precipitates in Ticolloy retarded the formation of $\delta$ by inhibiting the formation of a/2 ⟨110⟩ dislocations. The passage of these dislocations provides an easy mode for $\delta$ formation, but creates high-energy faults in the $\gamma'$. The energy required to generate these faults leads to a decrease in the rate of $\delta$ formation.[22] More recently, a new dual-superlattice superalloy reinforced by appreciable and comparable volume fractions of both $\gamma'$ and $\gamma''$ has been reported.[23,24] This alloy has been shown to possess excellent room and elevated temperature

P.M. MIGNANELLI, N.G. JONES, and H.J. STONE are with the Department of Materials Science and Metallurgy, 27 Charles Babbage Road, Cambridge, CB3 0FS, UK. Contact e-mail: hjs1002@cam.ac.uk M.C. HARDY is with the Rolls-Royce plc, PO BOX 31, Derby, DE24 8BJ, UK.

Manuscript submitted June 27, 2017.
Article published online October 5, 2017

strengths. In this work, we report on the time-temperature-transformation behavior of this new dual-superlattice superalloy and its age-hardenability following a range of thermal exposures.

## II. EXPERIMENTAL

A 500 g ingot, with a nominal composition of Ni-15Cr-4Al-6Nb (at. pct), was produced by vacuum induction melting from pure elements and solution heat treated above the $\gamma'$ solvus at 1473 K (1200 °C) for 4 hours in a vacuum. The composition of the alloy was measured by inductively coupled plasma–optical emission spectroscopy (ICP–OES) at IncoTest, UK. Following homogenization, the ingot was sectioned into ~1 $cm^3$ samples and heat treated for durations of 1 to 1000 hours at temperatures between 873 K and 1173 K (600 °C and 900 °C) in argon backfilled quartz ampoules. Differential scanning calorimetry (DSC) was conducted in a Netzsch 404 high-temperature calorimeter at a heating and cooling rate of 10 K $min^{-1}$ under flowing argon. The samples were mechanically ground and polished with diamond suspension to a 0.25-$\mu$m finish prior to electrolytic etching with a 10 vol. pct phosphoric acid solution at ~3 V. Secondary electron imaging (SEI) was completed using a JEOL 6340 FEGSEM and a FEI Nova NanoSEM 450. Synchrotron X-ray diffraction (XRD) patterns were obtained using the I12 beamline at the Diamond Light Source, Didcot, UK. The incident beam had an energy of 79.98 keV and dimensions of 0.5 × 0.5 mm. The samples were continuously heated using an electro-thermal mechanical tester, while diffraction data were acquired every ~1.5 K using a Pixium area detector. Analyses of the diffraction data were performed using Wavemetrics Igor Pro. Hardness measurements were made using a Vickers indenter with a 10 kg load and a 30 s dwell. Ten measurements were performed on each sample from which the mean hardness is reported along with the standard deviation.

## III. RESULTS

The actual composition of the alloy was measured by ICP–OES and determined to be 75.16 Ni—14.62 Cr—4.16 Al—6.06 Nb (at. pct), which was in good agreement with the nominal composition.

Microstructural examination of the thermally exposed samples was completed using SEI and representative images of the intragranular precipitates are presented in Figure 1. The SEI micrographs show that, for all of the thermal exposure conditions considered, $\gamma'$ had precipitated and was present in similar volume fractions (~25 to 30 pct) across the range of temperatures and exposure times considered. In the samples exposed at 873 K (600 °C), only $\gamma$ and $\gamma'$ phases were observed in the microstructure across the entire range of exposure times. However, after 1000 hours at 873 K (600 °C), an uneven surface relief was visible in the $\gamma$ matrix. Exposure of the alloy for 1 or 10 hours at 973 K (700 °C) produced $\gamma - \gamma'$ structures similar to those obtained following exposure at 873 K (600 °C). However, after 100 hours at 973 K (700 °C), fine laths were observed in the microstructure. The laths appeared to form between the $\gamma'$ precipitates in orientations parallel with the faces of the cuboidal $\gamma'$. With increased exposure time from 100 hours to 1000 hours at 973 K (700 °C), these laths appeared to coarsen. During heat treatment at 1023 K (750 °C), the laths precipitated and coarsened more rapidly than at lower temperatures, being initially observed after 10 hours and coarsening significantly following longer exposures. The precipitation and coarsening kinetics were further increased upon exposure at 1073 K (800 °C), with the laths being clearly visible after 1 hour and a large extent of coarsening occurred between 10 and 100 hours at this temperature. Following 1000 hours at 1073 K (800 °C), the fine laths were no longer visible within the microstructure, but larger laths were observed across the micrograph. These larger laths exhibited a different orientation relationship with the $\gamma'$ precipitates than the finer laths seen at the shorter exposure times and lower exposure temperatures, suggesting that they are a different phase. Following short exposures of 1 and 10 hours at 1173 K (900 °C), a $\gamma - \gamma'$ microstructure was observed, with no fine laths in the microstructure. However, after 100 hours, the large laths crossing the microstructure were again observed, accompanied by a decrease in the $\gamma'$ volume fraction.

To identify the phases present, synchrotron X-ray diffraction data were acquired from the samples exposed for 1000 hours at 873 K, 973 K, and 1073 K (600 °C, 700 °C, and 800 °C), Figure 2. The diffraction data obtained from all samples investigated contained reflections corresponding to a $\gamma$ matrix and $\gamma'$ precipitates. Notably, the sample exposed at 873 K (600 °C) exhibited a large asymmetry in the fundamental reflections, which is most apparent as a pronounced shoulder on the {311} $\gamma$ reflection (~7.5 deg 2$\theta$). This asymmetry is consistent with the presence of the $\gamma''$ phase, as the $c$ axis of the $\gamma''$ possess a lattice parameter greater than twice that of the lattice parameter of the cubic $\gamma$ and $\gamma'$, which manifests as a smaller diffraction angle for the {312} $\gamma''$ fundamental reflection than the {311} $\gamma$. The sample exposed for 1000 hours at 973 K (700 °C) showed clearly identifiable isolated reflections corresponding to the $\gamma$, $\gamma'$, and $\gamma''$ precipitates. The superlattice reflections of the two precipitates were well defined throughout the patterns and the shoulders on the fundamental reflections observed at 873 K (600 °C) became distinct peaks. Following exposure for 1000 hours at 1073 K (800 °C), large laths were visible in the micrograph, Figure 1(p), and the diffraction data corresponding to this condition exhibited distinct reflections consistent with the $\delta$ phase. The most pronounced reflections associated with this phase were the {012} and {211} at ~4.3 deg 2$\theta$, the {221} reflection at ~5.4 deg 2$\theta$, and the {400} at ~6.8 deg 2$\theta$. These are distinct from the $\eta$ phase, observed recently in some high Nb alloys,[25,26] as the $\eta$ phase does not exhibit a doublet at ~4.3 deg 2$\theta$, while the {023} reflection that is exhibited by the $\eta$ phase at ~4.7 deg 2$\theta$ is absent in the pattern presented below.

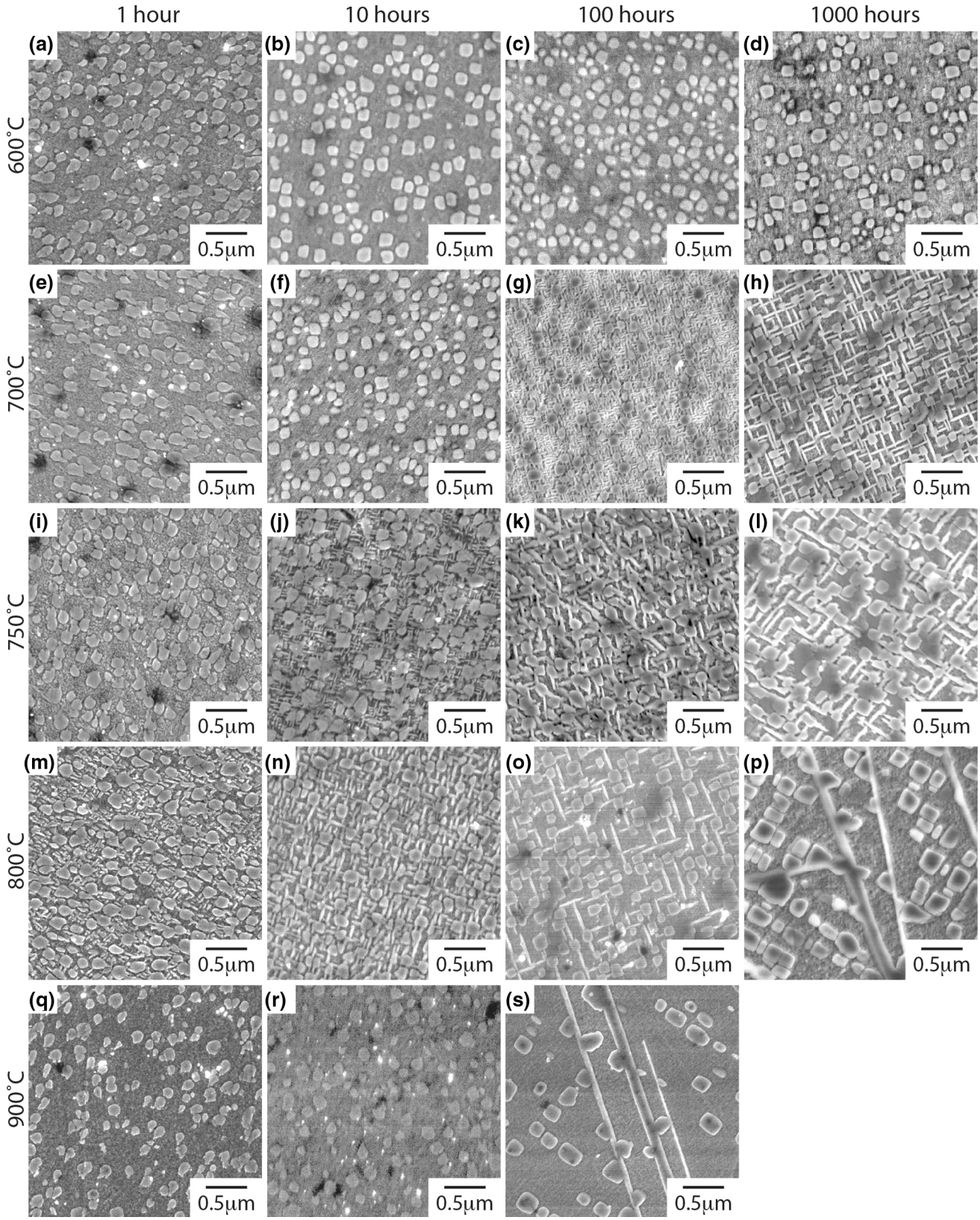


Fig. 1—SEI micrographs of the alloy following thermal exposure at 873 K (600 °C) for (*a*) 1 h, (*b*) 10 h, (*c*) 100 h, and (*d*) 1000 h; 973 K (700 °C) for (*e*) 1 h, (*f*) 10 h, (*g*) 100 h, and (*h*) 1000 h; 1023 K (750 °C) for (*i*) 1 h, (*j*) 10 h, (*k*) 100 h, and (*l*) 1000 h; 1073 K (800 °C) for (*m*) 1 h, (*n*) 10 h, (*o*) 100 h, and (*p*) 1000 h; 1173 K (900 °C) for (*q*) 1 h, (*r*) 10 h, and (*s*) 100 h.

However, despite the apparent transformation of $\gamma''$ to the thermodynamically stable $\delta$ phase, reflections corresponding to the $\gamma''$ phase could be identified. This indicated that even following a 1000-hour exposure at 1073 K (800 °C), $\gamma''$ precipitates persisted in the microstructure.

The DSC thermograms obtained from samples heat treated for 100 hours at 873 K, 973 K, and 1173 K (600 °C, 700 °C, and 900 °C), corresponding to microstructures comprising, $\gamma$- $\gamma'$, $\gamma$- $\gamma'$- $\gamma''$, and $\gamma$- $\gamma'$-$\delta$, respectively, are shown in Figure 3. In all cases, a single endothermic event was observed below the solidus temperature in the range 1173 K to 1323 K (900 °C to 1050 °C). While multiple endothermic events would be expected, associated with the dissolution of the precipitate phases, the close proximity of their solvus temperatures resulted in overlapping signals that prohibited their individual determination. Even if it were possible to discriminate between the different endothermic events, these could not be ascribed to the dissolution of a particular precipitate phase without corroborating metallographic studies. Despite this limitation, it was possible to evaluate each thermogram to obtain the maximum transition temperature observed, all of which occurred at 1288 K (1015 °C). As this temperature was consistent across the three different microstructural conditions tested, it was concluded that this temperature corresponded to the $\gamma'$ solvus.

In order to identify the individual solvus temperatures for the $\gamma''$, $\gamma'$, and $\delta$ phases, diffraction data were acquired while the dual-superlattice material was heated *in situ* at the Diamond Light Source, Figure 4. The reduced dataset showing the evolution of the desired phases (along with MC carbide) is presented in Figure 4(a), at a resolution of one diffractogram every 50 K. The temperature dependence of individual reflections that contained characteristic components of the $\gamma''$, $\gamma'$, and $\delta$ phases are provided in Figure 4(b through d) with a thermal resolution of 1.5 K. The dissolution of the $\gamma'$ phase, observed in Figure 4(c) as a decrease in the intensity of the {133} $\gamma'$ reflection, which can be seen as a shoulder at ~9.72 deg 2$\theta$ to the {133} $\gamma$ reflection at ~9.74 deg 2$\theta$, correlated well with the previous interpretation of the DSC data.

To determine the solvus temperatures of the $\gamma''$ and $\delta$ phases, the diffraction data shown in Figure 4 were analyzed using a multiple peak fitting routine and the resulting temperature dependence of the peak areas are shown in Figure 5. In each case, during heating, the peak area reduced gradually to a temperature ~150 K below the solvus temperature. Beyond this point, the peak area decreased rapidly, indicating considerable dissolution of the precipitate, which approached zero at the solvus temperature. The results of these analyses indicated that the solvus temperature of the $\gamma''$ phase was ~1200 K (927 °C) and that of the $\delta$ phase was ~1466 K (1193 °C).

Preliminary mechanical property data across the range of thermal conditions were acquired by room temperature hardness measurements. The hardness values obtained as a function of exposure time and temperature are shown in Figure 6. The samples exposed at 873 K (600 °C) showed increasing hardness with longer exposure times. However, the rate of increase in hardness was considerably steeper from 10 to 100 hours, which may be associated with the onset of $\gamma''$ precipitation in the alloy. This hypothesis is supported by shoulders on peaks in the X-ray diffraction data, Figure 2, consistent with the presence of the $\gamma''$ phase. Exposures at 973 K (700 °C) accelerated the precipitation kinetics and led to a peak hardness after 500 hours. This was followed by a small decrease in hardness of ~15 Hv after exposure for 1000 hours, showing excellent retention of properties. Initially, the response of the alloy to thermal exposure at 1023 K and 1073 K (750 °C and 800 °C) appeared to be very similar. The alloys exhibited nearly identical hardness values after 1 hour, which increased to a maximum after 10 hours, with the 1023 K (750 °C) having a greater

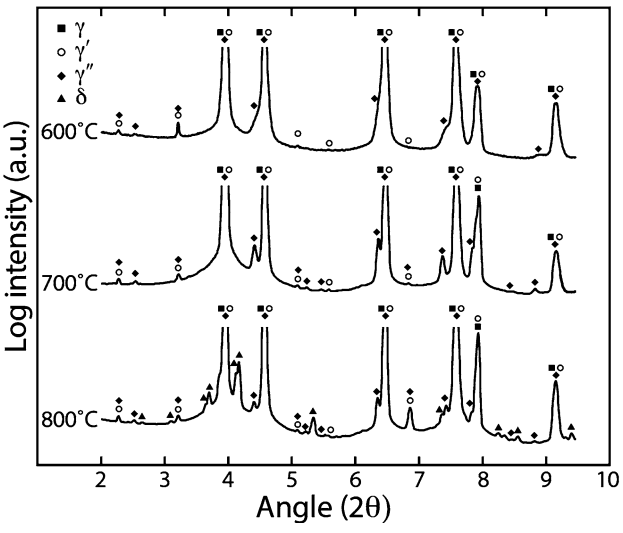


Fig. 2—Synchrotron X-ray diffraction data identifying the phases present in the alloy exposed for 1000 h at 873 K, 973 K, and 1073 K (600 °C, 700 °C, and 800 °C).

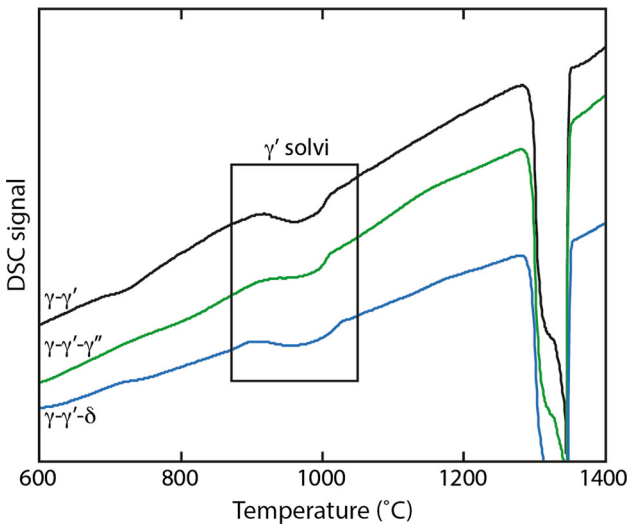


Fig. 3—DSC thermograms obtained on heating samples of the alloy with microstructures comprising, $\gamma$- $\gamma'$, $\gamma$- $\gamma'$- $\gamma''$, and $\gamma$- $\gamma'$-$\delta$.

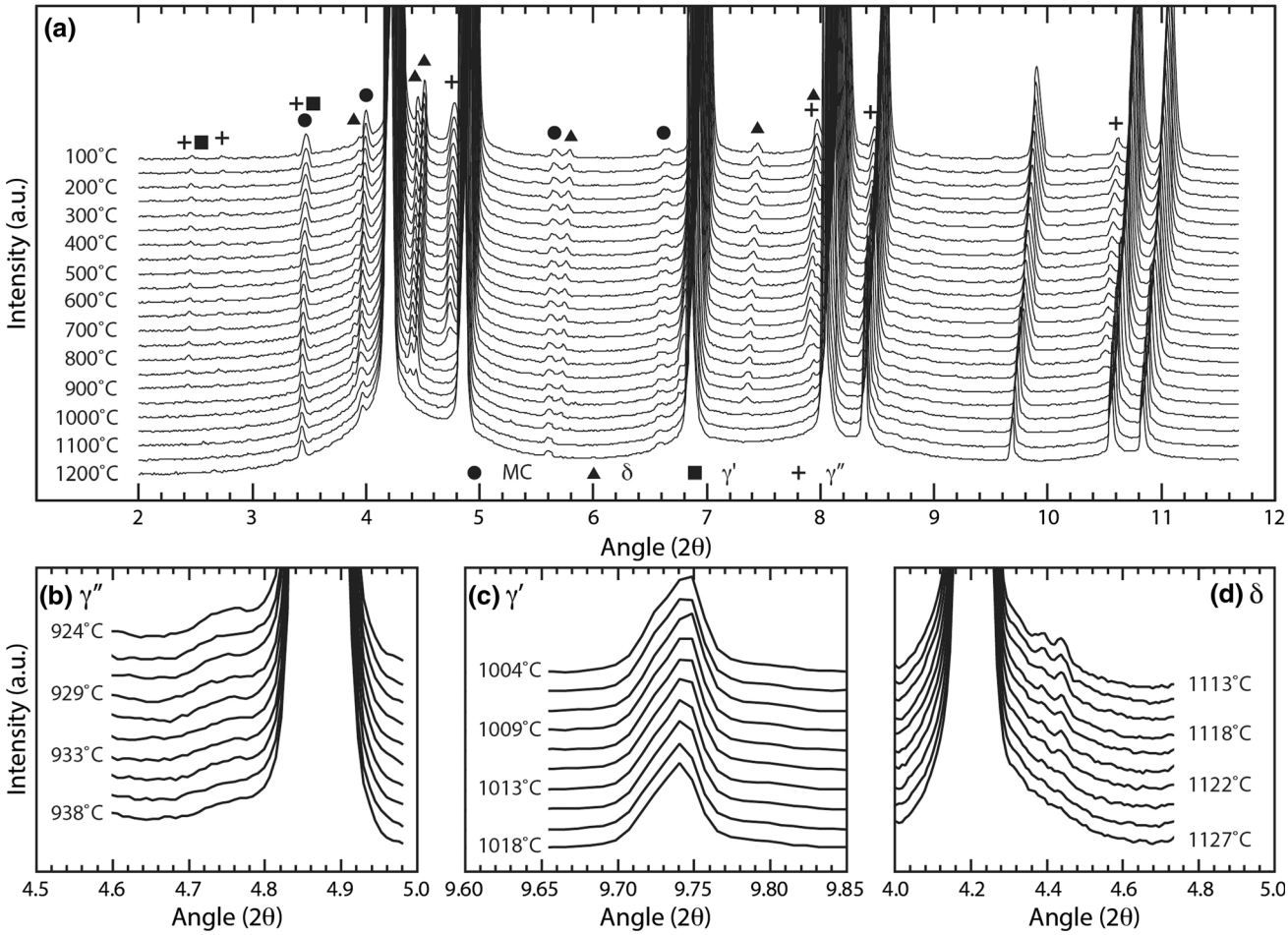


Fig. 4—Synchrotron X-ray diffraction data obtained during heating of the dual-superlattice superalloy. (*a*) Overview of the diffraction data obtained from 373 K to 1473 K (100 °C to 1200 °C). Detailed regions around diffraction peaks that show the dissolution of the (*b*) $\gamma''$, (*c*) $\gamma'$, and (*d*) $\delta$ phases to ascertain their associated solvus temperatures.

value, and then showed a similar decrease between 10 and 100 hours. The difference in the properties for these two exposure temperatures occurred between the 500- and 1000-hour exposures, where the exposure at 1073 K (800 °C) produced a larger decrease in the hardness than the exposure at 1023 K (750 °C). The exposure at 1173 K (900 °C) exhibited a markedly different hardness response across the range of exposure times. At this temperature, the hardness was lower than those following all other exposures, but exhibited a small increase between 10 and 100 hours.

## IV. DISCUSSION

The use of scanning electron microscopy and synchrotron X-ray diffraction permitted the unambiguous identification of the phases present in the dual-superlattice nickel-based superalloy. This, in turn, has allowed the construction of a preliminary time-temperature-transformation (T-T-T) diagram encompassing the data points from thermal exposures of 1 to 1000 hours at temperatures between 873 K and 1173 K (600 °C to 900 °C) and lines schematically illustrating the division of the relevant phase fields, Figure 7. T-T-T data from (a) IN718 and (b) IN625 (solid lines), reported in the literature,[12,27] have also been included for comparison.

From Figure 7, it is apparent that the formation of the $\gamma'$ precipitates cannot be practically suppressed in the microstructure and that this phase remains the fastest intermetallic species to form, in line with conventional nickel-based superalloy metallurgy. The rate at which the $\gamma''$ precipitates form is more sluggish than that observed in IN718 and IN625 and varies markedly with thermal exposure temperature and time. It is thought that the prior precipitation of $\gamma'$ may be responsible for the sluggish $\gamma''$ kinetics, in comparison to the other alloys, although further work is required to verify this hypothesis. This is shown by the nose of the T-T-T curve, where $\gamma''$ precipitation occurs after 1 hour at 1073 K (800 °C), whereas decreasing the temperature by 100 K, to 973 K (700 °C), slows precipitation, such that 100 hours is required for $\gamma''$ formation. The slow precipitation kinetics of the $\gamma''$ reinforcing phase illustrates the age-hardenability of this new class of alloy and its amenability to property optimization through post-processing heat treatment. The highest volume fractions of $\gamma''$ precipitates were observed in the alloy following 100 hours at 973 K (700 °C) and 10

hours at 1023 K (750 °C). As may be expected, longer duration exposures resulted in coarsening of the precipitates. It is also possible that the kinetics of $\gamma''$ precipitation may be affected by prior processing and applied stress, although further studies would be required to ascertain the extent to which this occurs.

The $\gamma''$ phase is known to be metastable and will transform to the thermodynamically stable $\delta$ phase during prolonged exposure at elevated temperatures. For the dual-superlattice nickel-based superalloy, this transformation to the $\delta$ phase requires ~500 hours at 1073 K (800 °C) or ~100 hours at 1173 K (900 °C). Such transformation kinetics are far slower than those of IN718, which has been reported to precipitate the $\delta$ phase after ~1 hour at 1073 K (800 °C) or ~50 hours at 973 K (700 °C).[12] This demonstrates that the dual-superlattice superalloy possesses far superior microstructural stability than IN718. The sluggish transformation from $\gamma''$ to $\delta$ in the dual-superlattice superalloy may be related to the role of the substantial volume fraction of $\gamma'$ present. Collier, Selius, and Tien[28] proposed that the presence of $\gamma'$ precipitates inhibits the transformation of $\gamma''$ to $\delta$, as the dislocations that enable the easy transformation to $\delta$ introduce high-energy faults in the $\gamma'$ with an inherent energy penalty. Therefore, the relatively high volume fraction of $\gamma'$ in the dual-superlattice superalloy, greater than that of either IN718 or Ticolloy,[20] is thought to severely inhibit the precipitation of the $\delta$ phase, thereby stabilizing the $\gamma - \gamma' - \gamma''$ microstructure observed.

The hardness variation of the dual-superlattice superalloy with thermal exposure condition can be directly correlated with the microstructural trends observed previously. Thermal exposure at 873 K (600 °C) for 1 and 10 hours produces an alloy with a $\gamma$-$\gamma'$ microstructure and a low hardness. Longer exposures at 873 K (600 °C) generated a much greater hardening response and the alloy exposed for 1000 hours at 873 K (600 °C) had the greatest hardness at this temperature. This was attributed to the presence of precipitates of $\gamma''$ in the microstructure. The hardness of the sample exposed for 100 hours at 873 K (600 °C) is greater than that measured from other conditions with $\gamma - \gamma'$ microstructures, possibly indicating the onset of $\gamma''$ precipitation. While distinct $\gamma''$ precipitates were not observed in the SEI micrographs, the uneven surface relief observed may indicate the presence of extremely fine precipitates, beyond the resolution of the microscope used in this study.

As discussed previously, an increase in the thermal exposure temperature will increase the precipitation kinetics of the $\gamma''$ phase in this alloy. This produced peak hardness values after 500 hours at 973 K (700 °C), and following 10 hours at either 1023 K or 1073 K (750 °C or 800 °C). These values corresponded with the microstructures containing the finest $\gamma''$ laths for each exposure temperature. The strengthening contribution of $\gamma''$ in these alloys can clearly be seen from the rapid increase in the rate of hardening observed in conditions with microstructures containing the greatest proportions of the $\gamma''$ phase. It should be noted that the increase in hardness observed in the samples exposed at 1173 K

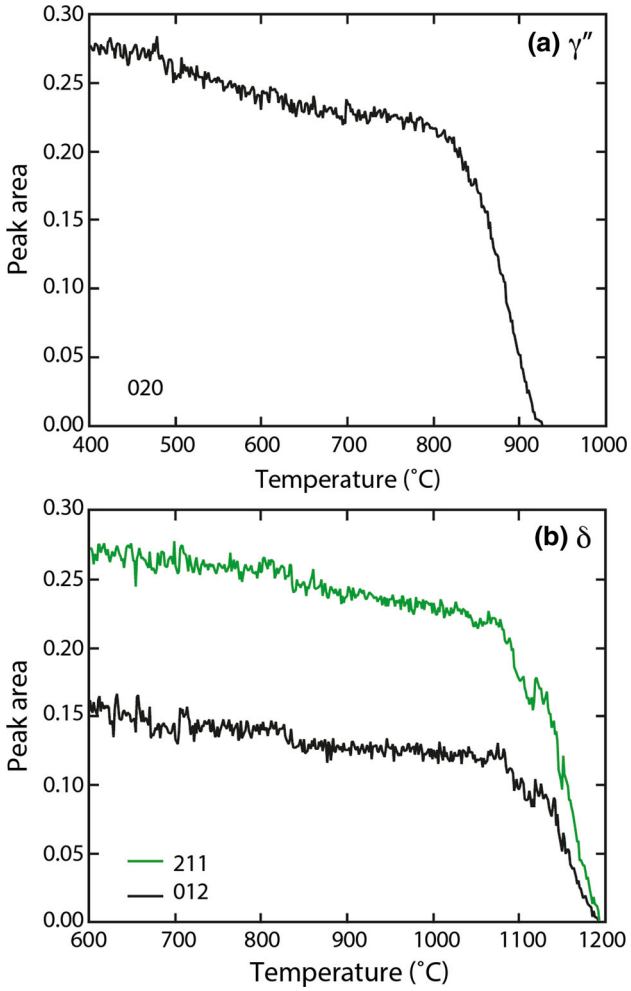


Fig. 5—Plots of the area of selected diffraction peaks as a function of temperature. (*a*) The {004} peak of the $\gamma''$ phase and (*b*) the {211} and {012} peaks of the $\delta$ phase.

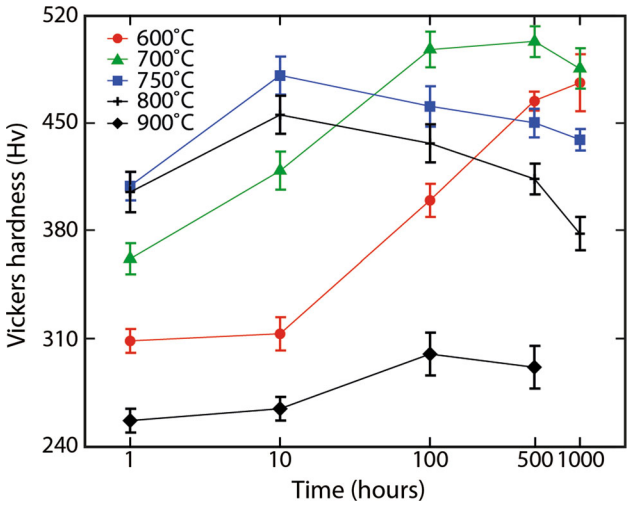


Fig. 6—Room temperature hardness data following thermal exposures between 873 K and 1173 K (600 °C and 900 °C) for 1 to 1000 h.

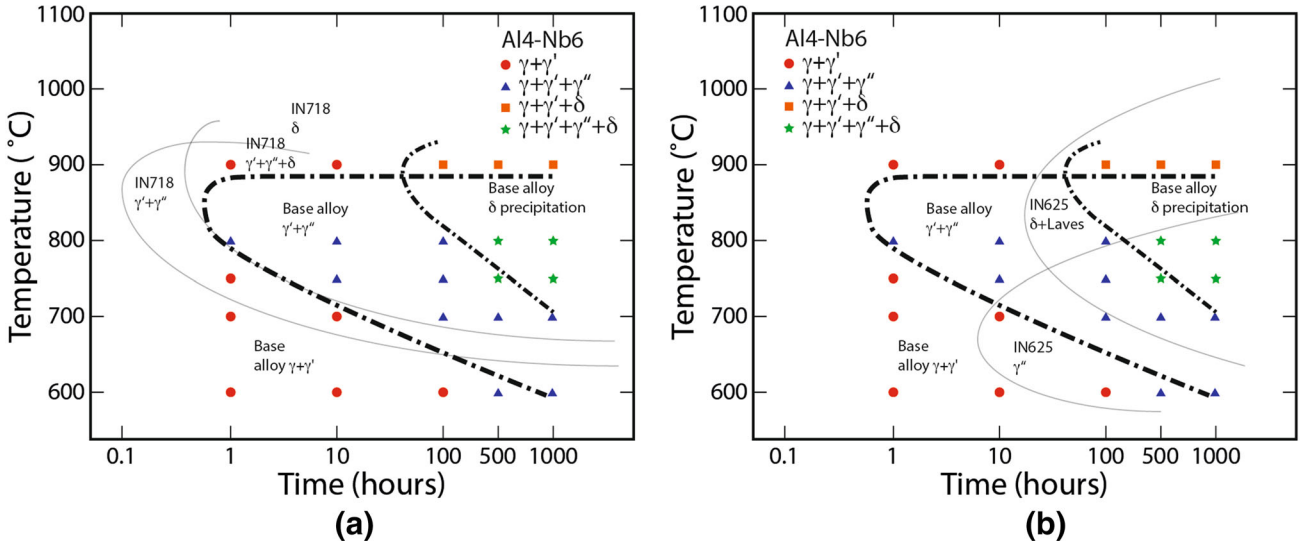


Fig. 7—T-T-T data for the new dual-superlattice superalloy, with the T-T-T diagram for (*a*) IN718[12] and (*b*) IN625[27] overlaid for comparison.

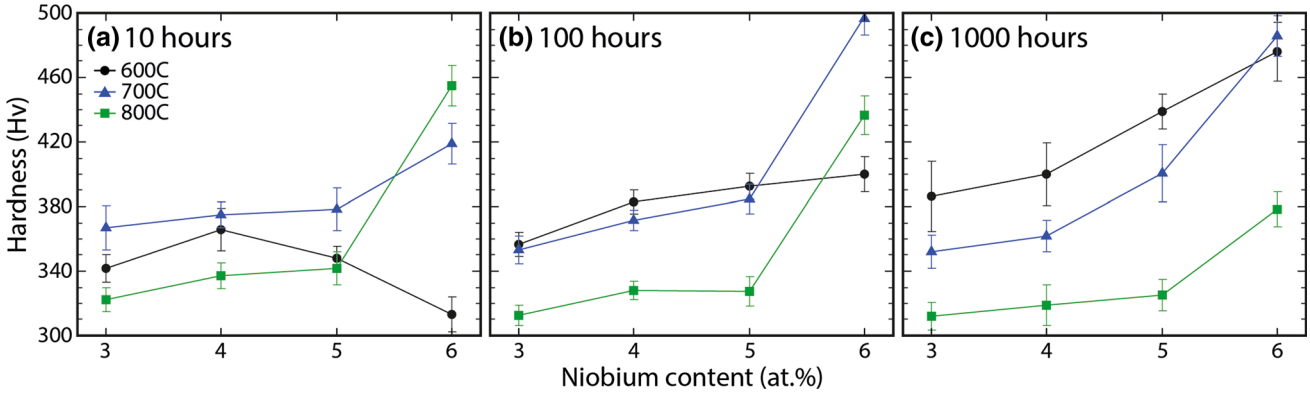


Fig. 8—The variation in hardness of Ni-15Cr-xAl-(10-x)Nb alloys with varying Nb content for exposures of *a*) 10 h, *b*) 100 h, and *c*) 1000 h at temperatures of 873 K, 973 K, and 1073 K (600 °C, 700 °C, and 800 °C).[29]

(900 °C), at times of 100 and 500 hours, could be ascribed to the precipitation of the $\delta$ phase. This, as a hard intermetallic phase, will initially increase the hardness of the alloy but be detrimental to many of the other properties critical to the effective use of nickel-based superalloys.

To further establish the hardening contribution from the $\gamma''$ phase, comparisons can be made with the hardness values of other Ni-15Cr-$x$Al-$(10-x)$Nb alloys[29] following exposures for 10, 100, and 1000 hours at 873 K, 973 K, and 1073 K (600 °C, 700 °C, and 800 °C), Figure 8. The alloys Ni-15Cr-7Al-3Nb, Ni-15Cr-6Al-4Nb, and Ni-15Cr-5Al-5Nb all had $\gamma$- $\gamma'$ microstructures and showed hardness values that increased only slightly with Nb content, dominated by changes in their $\gamma'$ sizes.[29] For the alloy in the current study, heat treatment conditions that generated a $\gamma$- $\gamma'$ microstructure exhibited hardness values comparable to those of the other Ni-Cr-Al-Nb alloys. In contrast, those microstructural conditions that precipitated the $\gamma''$ phase had greatly increased hardness values. This is most clearly evident in the exposure for 10 hours at 1073 K (800 °C) and for 100 hours at 973 K or 1073 K (700 °C or 800 °C), where a large increase in hardness of ~120 Hv is achieved in each case. Interestingly, after 1000 hours at 873 K (600 °C) and 973 K (700 °C), the Ni-15Cr-5Al-5Nb alloy possessed a hardness intermediate between those of the alloys with lower Nb concentration and that of the present study. This may indicate that the early onset of $\gamma''$ precipitation had occurred in Ni-15Cr-5Al-5Nb following these thermal exposures, which could not be identified with the techniques used in the previous study.[29]

The difference in the peak hardness between the sample exposed at 973 K (700 °C) for 100 hours and the sample exposed at 1023 K (750 °C) for 10 hours, Figure 6, indicates that the microstructure for maximum strength has not yet been identified. Investigation of further heat treatments, including two step aging heat treatments, to aid $\gamma''$ nucleation and growth, will be required to optimize the mechanical properties of this new alloy class.

The change in the microstructure brought about by overaging heat treatments resulted in a softening of the alloy as a result of the coarsening of the $\gamma''$ precipitates. After 1000 hours at 973 K (700 °C), this reduction is very small, indicating an excellent retention of mechanical properties at this temperature. However, a larger decrease in the hardness was observed after 1000 hours at 1023 K (750 °C). This correlates with the increased coarsening kinetics observed at this higher temperature. At 1073 K (800 °C), the hardness decreases rapidly between 100 and 1000 hours of exposure. This change in properties is associated with the transformation of the $\gamma''$ precipitates to the $\delta$ phase. However, as shown in the synchrotron X-ray diffraction data, the retention of a limited volume fraction of $\gamma''$ ensures that the hardness remains considerably greater than $\gamma''$-free microstructures of both similar alloys and the dual-superlattice alloy exposed at 873 K (600 °C) for 1 and 10 hours.

Further increases in the thermal exposure temperature to 1173 K (900 °C) produced a microstructure with a very low hardness value, below that of the $\gamma - \gamma'$ 873 K (600 °C) samples. The origins of this hardness deficit are two-fold: Firstly, the $\gamma''$ solvus is known to be 1200 K (927 °C), and therefore, the exposure at 1173 K (900 °C) produces a microstructure that is devoid, or has minimal amounts, of the reinforcing $\gamma''$. Secondly, the elevated temperature decreases the volume fraction of the $\gamma'$ precipitates in the alloy as the $\gamma'$ solvus is approached, which leads to a concomitant reduction in hardness.

## V. CONCLUSIONS

The precipitation behavior of a new dual-superlattice superalloy has been characterized using a combination of electron microscopy and synchrotron X-ray diffraction following thermal exposures for durations of 1 to 1000 hours and temperatures between 873 K and 1173 K (600 and 900 °C). The $\gamma''$ precipitates in this new class of alloys have been shown to be stable at temperatures below 1023 K (750 °C) for up to 1000 hours. In contrast, exposure at 1073 K (800 °C) required durations in excess of 100 hours before the precipitation of $\delta$ was observed. This assessment has allowed the construction of a preliminary T-T-T diagram for this new class of alloys.

The variation in strength of the dual-superlattice superalloy with microstructural condition has been elucidated through using hardness as a proxy measurement. The formation of $\gamma''$ precipitates was seen to give rise to significant increases in the alloy hardness, while subsequent coarsening resulted in reduced values. Overaging to form $\delta$ or aging at 1173 K (900 °C) greatly reduced the hardness as result of the dissolution of the $\gamma''$ and the coarsening and reduced volume fraction of $\gamma'$.

## ACKNOWLEDGMENTS

The authors would like to thank K. Roberts and S. Rhodes for experimental assistance, and acknowledge funding through the EPSRC/Rolls-Royce strategic partnership EP/M005607/1 and EP/H022309/1 as well as from the Diamond Light Source for the provision of beam time (EE9270).

## OPEN ACCESS



## REFERENCES

1. F.R. Preli and D. Furrer: *8th International Symposium on Superalloy 718 and Derivatives*, 2014, pp. 3–14.
2. J.A. Heaney, M.L. Lasonde, A.M. Powell, B.J. Bond and C.M. O'Brien: *8th International Symposium on Superalloy 718 and Derivatives*, 2014, pp. 67–77.
3. K-M. Chang and A.H. Nahm, *Superalloy 718—Metallurgy and Applications*, 1989, pp. 631–46.
4. R.C. Helmink: *8th International Symposium on Superalloy 718 and Derivatives*, 2014, pp. 171–80.
5. W.J. Boesch and H.B. Canada: *International Symposium on Structural Stability in Superalloys*, 1968, pp. 579–96.
6. S. Hong, W. Chen, and T. Wang: *Metall. Mater. Trans. A*, 2001, vol. 32A, pp. 1887–1901.
7. C. Slama, C. Servant, and G. Cizeron: *J. Mater. Res.*, 1997, vol. 12, pp. 2298–2316.
8. M.C. Chaturvedi and Y.-F. Han: *Met. Sci.*, 1983, vol. 17, pp. 145–49.
9. D.F. Paulonis, J.M. Oblak, and D.S. Duvall: *ASM Trans. Q.*, 1969, vol. 62, pp. 611–22.
10. M. Sundararaman, P. Mukhopadhyay, and S. Banerjee: *Metall. Mater. Trans. A*, 1992, vol. 23A, pp. 2015–28.
11. M. Sundararaman, P. Mukhopadhyay, and S. Banerjee: *Metall. Trans. A*, 1988, vol. 19, pp. 453–65.
12. A. Oradei-Basile and J.F. Radavich: *Superalloys 718, 625 and Various Derivatives*, 1991, pp. 325–35.
13. Z.S. Yu, J.X. Zhang, Y. Yuan, R.C. Zhou, H.J. Zhang, and H.Z. Wang: *Mater. Sci. Eng. A*, 2015, vol. 634, pp. 55–63.
14. S.T. Wlodek and R.D. Field: *Superalloys 718, 625, 706 and Various Derivatives*, 1994, pp. 659–71.
15. R. Cozar and A. Pineau: *Metall. Trans.*, 1973, vol. 4, pp. 47–59.
16. R.L. Kennedy: *Superalloys 718, 625, 706 and Various Derivatives*, 2005, pp. 1–14.
17. W-D. Cao and R.L. Kennedy: *Tenth International Symposium on Superalloys*, 2004, pp. 91–99.
18. J.P. Collier, S.H. Wong, J.C. Phillips, and J.K. Tien: *Metall. Mater. Trans. A*, 1988, vol. 19A, pp. 1657–66.
19. E. Andrieu, N. Wang, R. Molins and A. Pineau: *Superalloys 718, 625, 706 and Various Derivatives*, 1994, pp. 695–710.
20. J.K. Tien, J.P. Collier, P.L. Bretz and B.C. Hendrix: *Proceedings of the 1990 high temperature materials for power engineering conference*, 1990, pp. 1341–56.
21. J.A. Manriquez, P.L. Bretz, L. Rabenburg and J.K. Tien: *Seventh International Symposium on Superalloys*, 1992, pp. 507–16.
22. J.M. Oblak, D.F. Paulonis, and D.S. Duvall: *Metall. Trans.*, 1974, vol. 5, pp. 143–53.
23. P.M. Mignanelli, N.G. Jones, E.J. Pickering, O.M.D.M. Messé, C.M.F. Rae, M.C. Hardy, and H.J. Stone: *Scr. Mater.*, 2017, vol. 136, pp. 136–40.
24. M.C. Hardy, H.J. Stone, N.G Jones and P.M. Mignanelli: US Patent Application US 2017/0022586A1, Jan. 26 2017.
25. E.J. Pickering, H. Mathur, A. Bhowmik, O.M.D.M. Messé, J.S. Barnard, M.C. Hardy, R. Krakow, K. Loehnert, H.J. Stone, and C.M.F. Rae: *Acta Mater.*, 2012, vol. 60, pp. 2757–69.

26. O.M.D.M. Messé, J.S. Barnard, E.J. Pickering, P.A. Midgley, and C.M.F. Rae: *Phil. Mag*, 2014, vol. 94, pp. 1132–52.
27. S. Floreen, G.E. Fuchs and W.J. Yang: *Superalloys 718, 625, 706 and various derivatives*, 1994, pp. 13–37.
28. J.P. Collier, A.O. Selius and J.K. Tien: *Sixth International Symposium on Superalloys*, 1988, pp. 43–52.
29. P.M. Mignanelli, N.G. Jones, M.C. Hardy, and H.J. Stone: *Mater. Sci. Eng. A*, 2014, vol. 612, pp. 179–86.